Continental Shelf Research 30 (2010) 1314–1323

Contents lists available at ScienceDirect

Continental Shelf Research

journal homepage: www.elsevier.com/locate/csr

An idealized model study of flocculation on sediment trapping in an estuarine turbidity maximum

Fanghua Xu [a,*], Dong-Ping Wang [a], Nicole Riemer [b]

[a] School of Marine and Atmospheric Sciences, Stony Brook University, Stony Brook, New York, NY, USA
[b] Department of Atmospheric Sciences, University of Illinois at Urbana-Champaign, Urbana, IL, USA

ARTICLE INFO

Article history:
Received 13 March 2009
Received in revised form
25 December 2009
Accepted 30 April 2010
Available online 20 May 2010

Keywords:
Flocculation
Estuarine turbidity maximum
Tidal asymmetry
Numerical simulation

ABSTRACT

Flocculation has an important impact on particle trapping in estuarine turbidity maximum (ETM) through associated increases in particle settling velocity. To quantify the importance of the flocculation processes, a size-resolved flocculation model is implemented into an ocean circulation model to simulate fine-grained particle trapping in an ETM. The model resolves the particle size from robust small flocs, about 30 μm, to very large flocs, over 1000 μm. An idealized two-dimensional model study is performed to simulate along-channel variations of suspended sediment concentrations driven by gravitational circulation and tidal currents. The results indicate that the flocculation processes play a key role in generating strong tidal asymmetrical variations in suspended sediment concentration and particle trapping. Comparison with observations suggests that the flocculation model produces realistic characteristics of an ETM.

1. Introduction

An estuarine turbidity maximum (ETM) is a region of elevated suspended sediment concentrations (SSC) often located at the landward limit of the salt intrusion (salt front). An ETM is important for stratigraphy and estuarine ecosystem on both short and long time scales (Traykovski et al., 2004; Simenstad et al., 1994). Suspended sediment trapping at an ETM has been well documented, e.g. in the upper Chesapeake Bay (Schubel, 1968; Sanford et al., 2001), the Columbia River estuary (Jay and Musiak, 1994), and the Hudson estuary (Traykovski et al., 2004). For instance, Sanford et al. (2001) showed that in the upper Chesapeake Bay ETM sediment trapping was very efficient during a large flood event.

The mechanisms of particle trapping at an ETM are complex. In general, convergence at the salt front of landward sediment flux by the gravitational circulation and seaward sediment flux by the river flow is considered a fundamental mechanism contributing to ETM formation (Postma, 1967). In most estuaries, a spatially limited pool of resuspendable particles is found near the salt front (Sanford et al., 2001), and tidal resuspension has been recognized as a key factor in maintaining high SSC (Schubel, 1968). Tidal asymmetry also contributes to the ETM formation. Tidal currents generally are surface intensified at ebb but are bottom intensified at flood. Also, vertical mixing is suppressed at ebb but enhanced at flood, due to the interaction of vertically sheared tidal currents with the along-channel salinity gradients. Jay and Musiak (1994) discussed the tidal pumping, an upstream net transport of suspended sediments resulting from strong tidal asymmetry in stratification and flow field. Geyer (1993) showed that the suppression of turbulence by density stratification tends to keep the particles near bed at the convergence zone. Lateral interactions between currents and topography also have the potential to enhance asymmetric sediment trapping (Geyer et al., 1998).

A number of modeling studies of ETM have investigated the importance of the aforementioned physical mechanisms. Festa and Hansen (1978) showed that gravitational circulation could successfully trap particles independent of tidal forcing. Burchard and Baumert (1998) evaluated the relative influence of residual gravitational circulation, tidal velocity asymmetry, and tidal mixing asymmetry on ETM using an idealized two-dimensional (x–z) model. The first two mechanisms are found to be necessary for ETM formation, but the tidal mixing asymmetry does not appear to be essential. North et al. (2004) explored the effects of wind and river pulses on ETM. They found that during pulse events the salt front structure and circulation pattern were significantly influenced, and so were the transport and distribution of suspended sediments. Park et al. (2008) found that the mechanisms responsible for ETM formation were different between low and high flow conditions. For a low flow condition, an ETM is mainly formed by local erosion/deposition and convergence of horizontal bottom sediment flux, while for a high flow condition an ETM is produced by strong convergence of

* Corresponding author. Current address: Atmospheric and Oceanic Sciences (AOS), Princeton University, USA.
E-mail address: fxu@princeton.edu (F. Xu).

0278-4343/$ - see front matter © 2010 Elsevier Ltd. All rights reserved.
doi:10.1016/j.csr.2010.04.014

seaward sediment flux eroded from the upstream of the salt front and landward sediment flux settled near the salt front. Warner et al. (2007) tested the sensitivity of ETM formation to settling velocity, tidal mixing, and sediment supply. They found that a proper settling velocity was critical for ETM formation. In their experimental setup, at low settling velocity ($\sim$0.01 mm s^{-1}), particles would suspend long enough to escape from the estuary, whereas with high settling velocity ($\sim$0.5 mm s^{-1}), particles settle quickly upstream of the salt front and contribute little to the ETM.

Flocculation has been recognized as an important process for sediment trapping in estuaries (e.g. Geyer et al., 2004). In an ETM, particle size and settling velocity are continuously changing in response to environmental conditions. In situ observations of suspended sediments have shown that a large portion of fine-grained sediments are packed into flocs in turbid plumes. The floc size can range from a few micrometers to hundreds of micrometers, and flocculation can have a large impact on the transport and deposition of suspended particles in an ETM. For instance, in the Hudson estuary the particle size varied with tidal phases such that flocs became significantly larger (>250 μm) after maximum flood and ebb (Traykovski et al., 2004). In the York River estuary, the floc size also was found to vary with the tidal cycle (Scully and Friedrichs, 2007). Also, in Humber estuary, UK, a pronounced SSC near the bed was found at slack tides as a result of rapid settling of large flocs (Uncles et al., 2006).

Previous numerical model experiments have focused on effects of the tidal and residual circulation on the ETM formation. The cohesive sediments usually are treated as particles with constant one representative size or multiple sizes, and the variations in floc size due to aggregation and breakup processes of flocs with flow conditions are ignored. For example, Geyer et al. (1998) used one single size in their model study of the ETM in the lower Hudson River, and Park et al. (2008) used three separate size classes of fine, medium, and coarse particles to simulate of the ETM in the upper Chesapeake Bay. Alternatively, the flocculation process is included implicitly through changes in the settling velocity of fine sediments with SSC and turbulence field (e.g. Mehta, 1986; Lick et al., 1993; Van Leussen, 1994). Baugh and Manning (2007) implemented an empirical floc settling velocity to simulate sediment transport in the Lower Thames estuary, UK. Xie et al. (2009) used an empirical relation of settling velocity with the SSC to study sediment transport in Hangzhou Bay, China. Also, Winterwerp (1998, 2002) developed a semi-empirical flocculation model based on a collision efficiency function and a floc breakup function to predict a characteristic floc size with flow turbulence. The settling velocity is scaled as a function of the characteristic floc size and a fixed fractal dimension. Son and Hsu (2008) improved the Winterwerp's model using variable fractal dimensions.

We have developed a size-resolved flocculation model to predict temporal evolution of full floc size spectrum (Xu et al., 2008). The size-resolved flocculation model calculates settling velocity directly from the predicted size spectrum. In a one-dimensional (1-D) model study considering the particle flocculation, settling, deposition, and erosion, the model results revealed a large variation in floc size over a tidal cycle, consistent with the size distributions typically observed in an ETM. In this study, to explore further the effects of flocculation on ETM formation, we implement the size-resolved flocculation model into the Princeton Ocean Model (POM), and perform numerical experiments of an idealized estuary in a two-dimensional (x–z) channel. We use the Chesapeake Bay ETM as a prototype. Our focus is to investigate the influence of flocculation on ETM and to quantify the different processes that determine the sediment budget during a tidal cycle. The article is organized as follows: Section 2 presents a description of the flocculation scheme and the coupled sediment transport model. Section 3 describes the idealized experiments. We conclude in Section 4.

2. Model description and the experiment setup

2.1. The flocculation scheme

The flocculation scheme has been introduced and tested in our previous work (Xu et al., 2008). Following Xu et al. (2008), we discretize the size distribution of sediment particles into a number of size sections or bins. The following flocculation equation describes the rate of change of mass density including aggregation and breakup:

$$\frac{\partial g(y,t)}{\partial t} = \frac{1}{2}\int_{y_0}^{y} \frac{m^2}{m_c^2 m'} g(y_c,t)K(y_c,y')g(y',t)dy' - \int_{y_0}^{\infty} \frac{1}{m'} g(y,t)K(y,y')g(y',t)dy' + \int_{y_0}^{\infty} \frac{m}{m'} Q(y,y')P(y')g(y',t)dy' - \frac{1}{3m^2} g(y,t)P(y). \quad (1)$$

where $g(y,t)$ is the mass density as a function of time t and y, y is the logarithm of particle radius r with mass m, y_0 represents the first bin, $m_c=m-m'$, $y_c=y-y'$, K is the aggregation kernel describing the rate of particle contacts, P is the breakup kernel due to turbulent shear, and Q represents the number density function for the fragments formed by the breakup of a parent particle of mass m'. To denote the mass concentration in each bin, C_j ($=g_j d\ln r$) is used. The sum of C_j over all bins is the SSC.

The aggregation is due to turbulent shear and differential settling. The rectilinear aggregation kernel is $K=\alpha(K_{ts}+K_{ds})$, where α is the particle stickiness, and the kernels K_{ts} and K_{ds} estimate the collision rate per unit volume caused by turbulence shear and differential settling. α is assumed constant for all particle sizes for simplicity. The kernels K_{ts} and K_{ds} are given by

$$K_{ts} = \frac{4}{3} G(r_i+r_j)^3 \quad (2)$$

and

$$K_{ds} = 5\pi(r_i+r_j)^2 |w_{s,i}-w_{s,j}| \quad (3)$$

where r_i and r_j are the floc radius, $w_{s,i}$ and $w_{s,j}$ are the settling velocity of flocs in bins i and j. The shear rate is defined as $G=\sqrt{\varepsilon/\nu}$, where ε is the turbulent dissipation rate and ν is the kinematic viscosity of fluid. The settling velocity is calculated as a function of particle size from Sternberg et al. (1999)

$$w_{s,j} = 347.5602(2r_j)^{1.54}, \quad (4)$$

where r_j is in m and $w_{s,j}$ is in m s^{-1}. In Eq. (3), the coefficient 5 is used to include the fact that irregular floc shapes can increase the efficiency of floc contacts. The choice of the empirical constants has been verified with a lab experiment (Xu et al., 2008).

The binary breakup is used in the present study. Q is defined as

$$Q = \begin{cases} 2 & (m = m'/2) \\ 0 & (m \neq m'/2) \end{cases}. \quad (5)$$

The breakup kernel, P, is a function of shear rate and floc size. Assuming a fractal treatment, the breakup frequency can be written as (Winterwerp, 1998)

$$P_i = E\sqrt{\frac{\mu}{F_y}} G^{1.5}(2r_i)\left(\frac{r_i-r_1}{r_1}\right)^{3-n_f} \quad (6)$$

where μ is the dynamic viscosity, n_f is the fractal dimension, and $F_y \approx 10^{-10}$ Pa is the estimated yield strength. The fractal dimension of flocs is defined as (Winterwerp, 2002)

$$n_f = \lim_{L\to\infty} \frac{\ln(N(L))}{\ln(L)} \tag{7}$$

where $N(L)$ is the number of self similar primary particles and L is the linear particle size. n_f=2.0 is applied in calculating breakup kernel.

2.2. Sediment transport model description and model setup

The Princeton Ocean Model (POM) (Blumberg and Mellor 1987; Mellor 1998) is a hydrostatic, primitive equation ocean model and has been used extensively in estuarine circulation studies (e.g. North et al., 2004; Wang, 2006). To simulate suspended sediment flocculation and transport processes, the size-resolved flocculation scheme and a sediment transport component are implemented into POM. The Upper Chesapeake Bay ETM is used as a model prototype. The parameters interpreted from Sanford et al. (2001) are listed in Table 1. We configure an idealized estuary as a flat-bottom, rectangular channel of 25 km long, 1 km wide, and 12 m deep. The model's horizontal resolution is 1 km and there are 16 uniform sigma levels (vertical resolution is ~0.8 m). Lateral variations are not considered. At the two open ends, a constant river discharge plus a barotropic, semidiurnal (12 h) tidal forcing is specified, $\overline{u} = -0.1 + 0.4\sin(2\pi t/T)(\mathrm{m\,s^{-1}})$. Radiation conditions are used for the outgoing disturbances. The initial condition includes a longitudinal salinity gradient, $s(x) = 5(1+\tan\mathrm{h}(0.2(L_x/2 + 5000 - x)))$ (psu). At the open boundaries, the inflow salinity is specified at 0 psu at the river end and 10 psu at the ocean end.

The sediment transport model solves the equation for the mass concentration of each particle size bin

$$\frac{\partial C_j}{\partial t} + u\frac{\partial C_j}{\partial x} + w\frac{\partial C_j}{\partial z} - \frac{\partial w_{s,j} C_j}{\partial z} = \frac{\partial}{\partial z}\left(K_3 \frac{\partial C_j}{\partial z}\right). \tag{8}$$

where u and w are the longitudinal and vertical velocity, respectively, $w_{s,j}$ is the particle settling velocity in the bin j, and K_3 is the vertical eddy diffusivity. Eq. (8) describes the change in

Table 1
Observed parameters in July in the Upper Chesapeake Bay interpreted from Sanford et al. (2001).

Channel depth (m)	Estuarine circulation velocity ($\mathrm{m\,s^{-1}}$)	Background SSC ($\mathrm{kg\,m^{-3}}$)	Tidal currents amplitude ($\mathrm{m\,s^{-1}}$)	Longitudinal salinity gradient ($\mathrm{psu\,km^{-1}}$)	Bottom stratification on ebb ($\mathrm{km^{-1}}$)	Settling velocity ($\mathrm{mm\,s^{-1}}$)
12	0.2	0.03	0.4	0.5	0.5	0.3

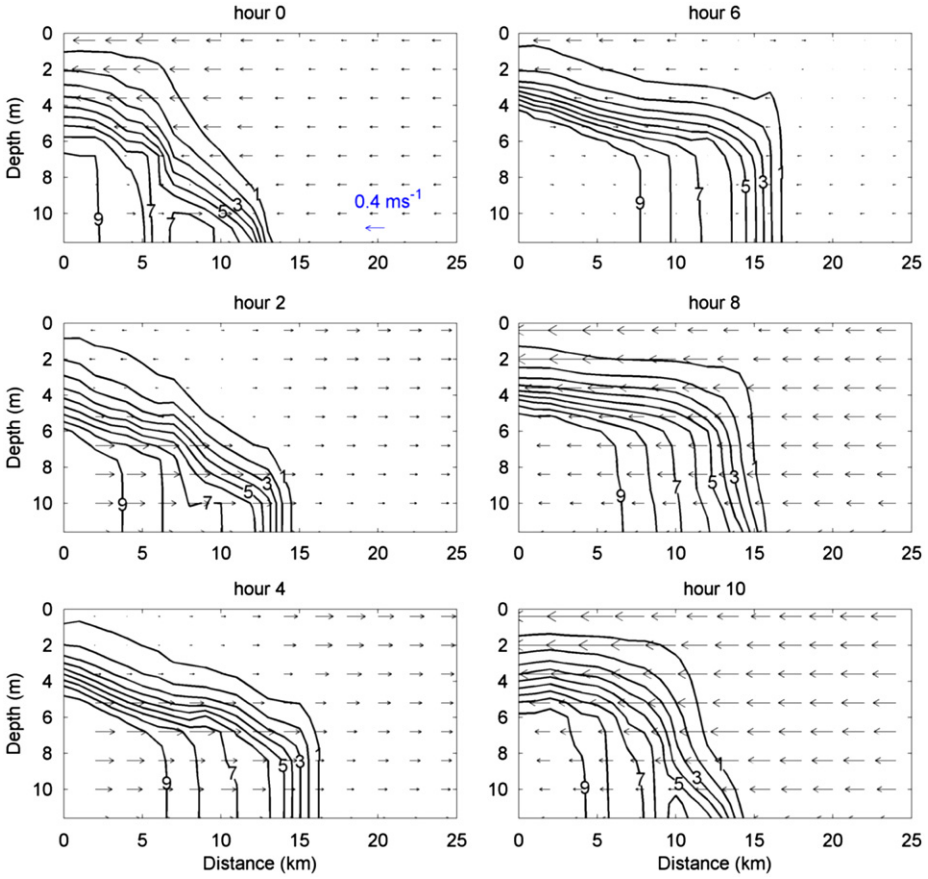

Fig. 1. Snapshots of along-channel salinity contours (solid lines; contour interval=1 psu) and velocity vectors from hour 0 to 10. The hour 0 denotes the slack before flood, and hour 6 denotes the slack before ebb.

SSC due to longitudinal and vertical advection, turbulent diffusion, and particle settling. A small horizontal diffusion is included only for numerical stability. The two velocity components (u and w) and the turbulence parameters (K_3 and ε) are provided by the circulation model. In POM the turbulence parameters are calculated based on the Mellor–Yamada level 2.5 turbulence closure (Mellor and Yamada, 1974). The particle mass flux from bottom erosion $E_{s,j}$ in bin j is described as

$$K_3 \frac{\partial C_j}{\partial z}\bigg|_{bottom} = E_{s,j} = E_{0,j}((\tau_b/\tau_c)-1)/j, \quad \text{when } \tau_b > \tau_c \tag{9}$$

where $E_{0,j}$ is a bed erodibility constant, assumed to be 1×10^{-3} kg m^{-2} s^{-1} for all size ranges. The bin number j in the denominator is used to account for the fact that larger particles are more difficult to erode than smaller ones (Xu et al., 2008). The bed shear stress $\tau_b = \rho C_d u\sqrt{u^2+v^2}$, where ρ is the reference density, 1025 kg m^{-3}. τ_c is the critical shear stress for erosion and is set to 0.05 Pa in the study (Warner et al., 2005). Considering the rapid tidal phase change, the consolidation process can be neglected (Uncles et al., 2006).

The sediment module is called at every internal step at the end of the circulation model update. First, the flocculation model (Eq. (1)) is solved using a time step, which typically is only a fraction of the circulation model's internal time step. After all the size bins are updated, the sediment transport model (Eq. (8)) is solved to redistribute the particles in space (including the sedimentation in the bed). Because of the large bin size and small time step, the flocculation model takes the bulk of the total model calculation.

The model starts from the rest, and reaches a quasi-periodic state in about 2 days. Then, a vertically well-mixed constant loading, 0.03 kg m^{-3}, of suspended primary particles of 30 μm, is imposed at the river end. These values are typical of the Chesapeake Bay background suspended sediments (Fig. 8 in Sanford et al. (2001) and Sanford et al. (2005)). The total bin number n is set to be 50. Thus, the size of flocs can vary in 30–1277 μm, which includes most of the floc size range in estuaries. The external and internal time steps for the circulation model are 5 and 50 s, respectively, and the time step for the flocculation model is 0.2 s. The SSC reaches a quasi-periodic state in about 3 days. For the flocculation model, results for day 7 are used in the analysis while for the non-flocculation model results for day 6 are used. For convenience, hour 0 denotes slack tide before flood, and hour 6 denotes slack tide before ebb. (Because the tidal period is 12 h, the phase is the same for both models.) Six simulation tests are carried out. Simulations with or without flocculation are to explore the influence of flocculation on sediment trapping. The other simulations test the sensitivity of the model on particle stickiness and fractal dimension.

3. Model results

3.1. Salinity and velocity

Fig. 1 illustrates along-channel variations in salinity and velocity from hour 0 to hour 10. The instantaneous flow field is a superposition of tidal currents and a steady gravitational circulation; the latter can be seen convergent at the salt front. The salt front, defined as 1 psu isohaline, moves back and forth with tidal currents between km 12 and 16. Upstream (landward) of the salt front the water column is fresh. Downstream of the salt front the salinity distributions vary with tidal currents. The effect of tidal straining is evident (Simpson et al., 2004). A well-developed bottom boundary layer capped by a sharp pycnocline is present at the end of flood. As the tide ebbs, the bottom boundary layer collapses, and strong stratification is present near the bottom. The horizontal salinity gradient at the salt front is about 0.5 psu km^{-1}, and the vertical salinity stratification is about 0.5 psu km^{-1} in the pycnocline. These values are comparable to those in the Upper Chesapeake Bay (Table 1).

Fig. 2 shows velocity profiles every 2 h at km 4 (estuary) and km 20 (river). At km 4, strong vertical shears are present during ebb as the tidal currents are enhanced by gravitational circulation. During flood tide, the gravitational circulation is evident in the strong bottom inflow. Also, at maximum flood (hour 4) a subsurface velocity maximum is present in the middle of the water column at the top of the bottom mixed layer. The strong tidal velocity asymmetry agrees well with observations in the

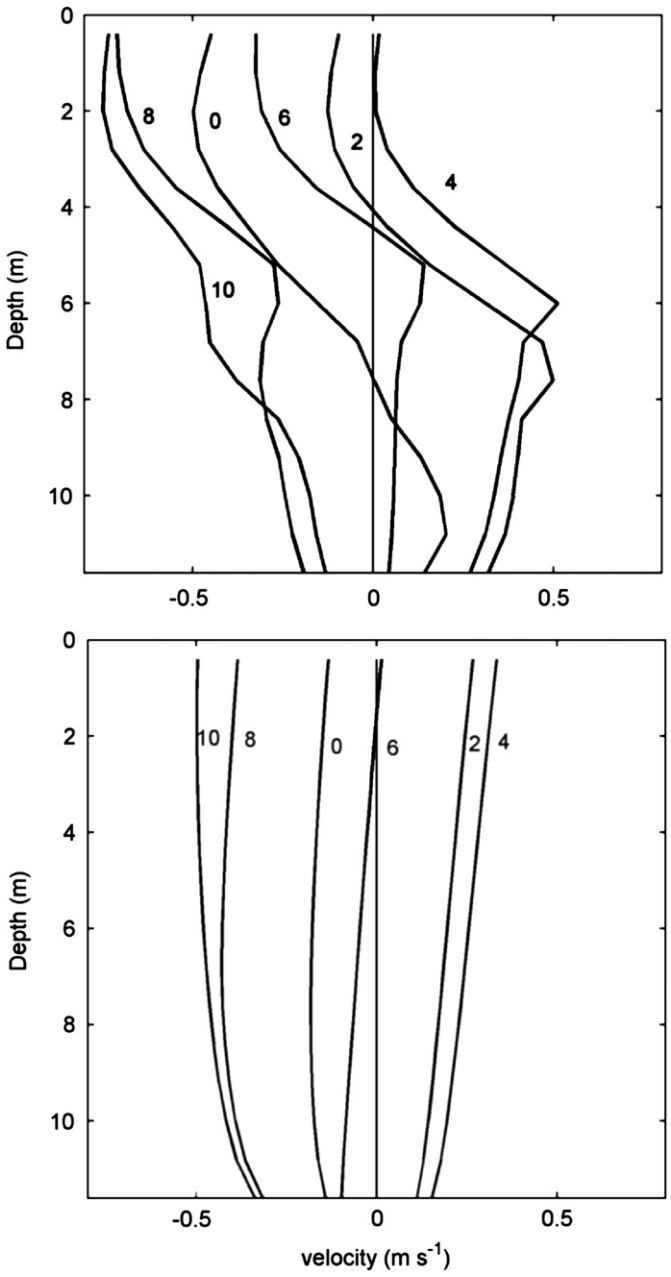

Fig. 2. Along-channel velocity profiles over a tidal cycle at $x=4$ km (upper panel) and $x=20$ km (lower panel). The time (in hour) is marked in each profile. Positive velocities are flood. The hour 0 denotes the slack before flood, and hour 6 denotes the slack before ebb.

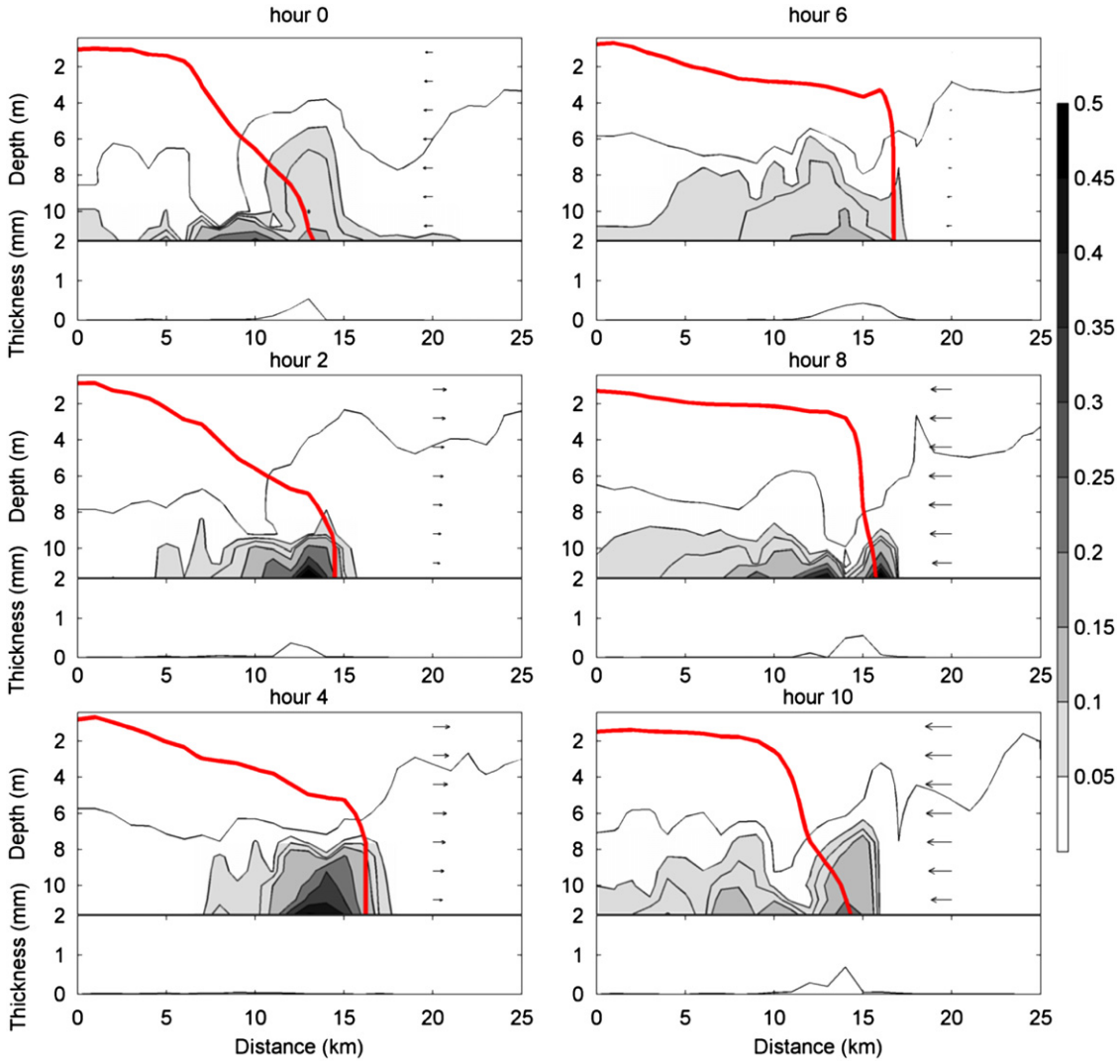

Fig. 3. Instantaneous SSC distributions with contours of 0.03, 0.05, 0.07, 0.1, 0.2, 0.3, and 0.4 kg m^{-3} (solid lines) and bottom thickness (blue line) from hour 0 to 10 with flocculation. The red line is 1 psu isohaline, and the arrows show the currents at km 20. (For interpretation of the references to color in this figure legend, the reader is referred to the web version of this article.)

Hudson River (Chant and Wilson, 2000; Trowbridge et al., 1999). At km 20, the tidal currents are relatively homogeneous with slight vertical shears near the bottom.

3.2. Simulation with the size-resolved flocculation model

The base case is a simulation with the size-resolved flocculation model. The particle stickiness α is fixed at 0.6. Fig. 3 shows snapshots of 1 psu isohaline, SSC and bed thickness distributions; the salinity distribution and velocity structure are the same as shown in Fig. 1. The bed thickness is defined as the amount of bottom sediments divided by the density of particles ρ_f and the total bed surface area. The SSC and its along-channel distributions show large tidal variations. At slack tide before flood (hour 0), the SSC is relatively low, about 0.1 kg m^{-3}. The ETM becomes prominent at the flood tide (hour 2 and 4) when SSC increases to >0.4 kg m^{-3}. The cycle repeats for the ebb cycle. However, the maximum SSC is significantly less at the ebb tide (hour 8), about 0.2 kg m^{-3}. In other words, the SSC has strong asymmetry between flood and ebb. Also, the center of the ETM is slightly upstream of the salt front at ebb (at hour 10), while it is further downstream at flood (hour 2 and 4). The fact that the ETM is behind the salt front in the direction of tidal flow is due to the tidal resuspension lag in that erosion takes place only after tidal velocity exceeds the critical shear stress (Dyer and Evans, 1989).

Sediment deposition occurs continuously while resuspension only occurs when the bottom shear stress exceeds the critical shear stress. The accumulation of sediments near the salt front is estimated by the bed thickness (Fig. 3). A sediment pool is formed following the salt front. There is strong variability of resuspension and deposition within a tidal cycle. On strong flood currents (hour 4), most particles are resuspended, resulting in the large SSC increase. In contrast, on strong ebb currents (hour 8), there is relatively small change in the bed thickness, and the SSC increase is mainly due to trapping of suspended sediments. Also, on ebb currents, the ETM zone spreads much further downstream from the salt front.

Fig. 4 shows longitudinal distributions of median floc size (D_{50}). The background median particle size is about 50 μm. Large flocs (>100 μm) are formed near the salt front due to convergence of suspended particles. At hour 0, the maximum D_{50} is about 150 μm seaward of the salt front despite the low SSC ($\sim$0.07 kg m^{-3}). In the subsequent flood tide, although the SSC is increasing, the median floc size is still about 150 μm (hour 2 and

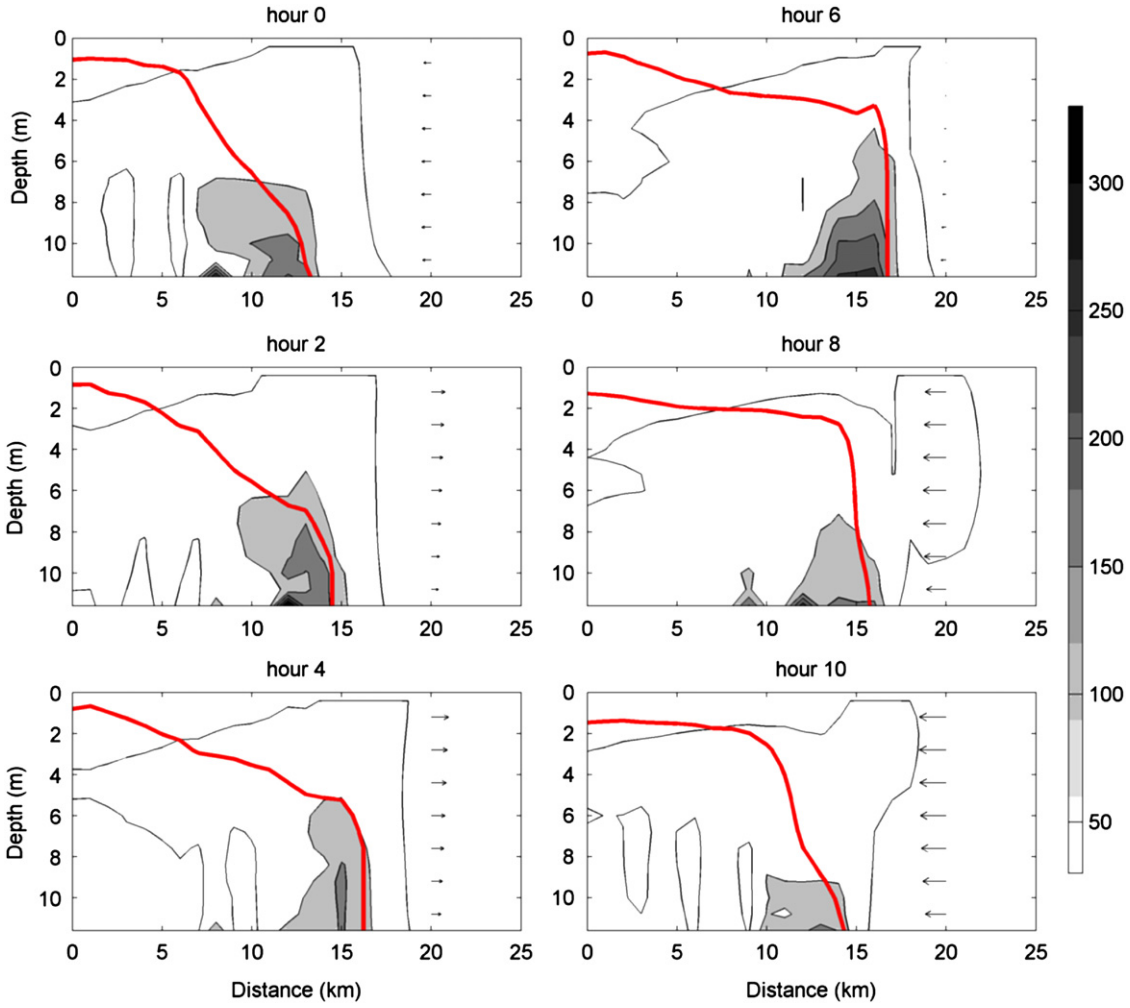

Fig. 4. Instantaneous median floc size (D_{50}) contours (50 μm interval) from hour 0 to 10 with flocculation. The background D_{50} is about 50 μm. The red line is 1 psu isohaline, and the arrows show the currents at km 20. (For interpretation of the references to color in this figure legend, the reader is referred to the web version of this article.)

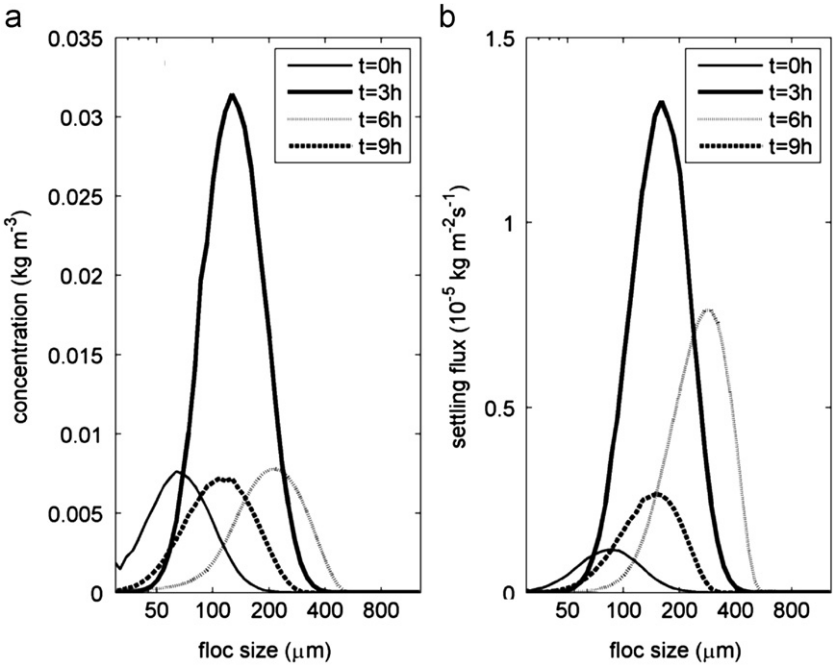

Fig. 5. Left: floc size distributions of mass concentration. Right: settling flux of flocs at different tidal phases at 0.8 mab, $x=14.5$ km.

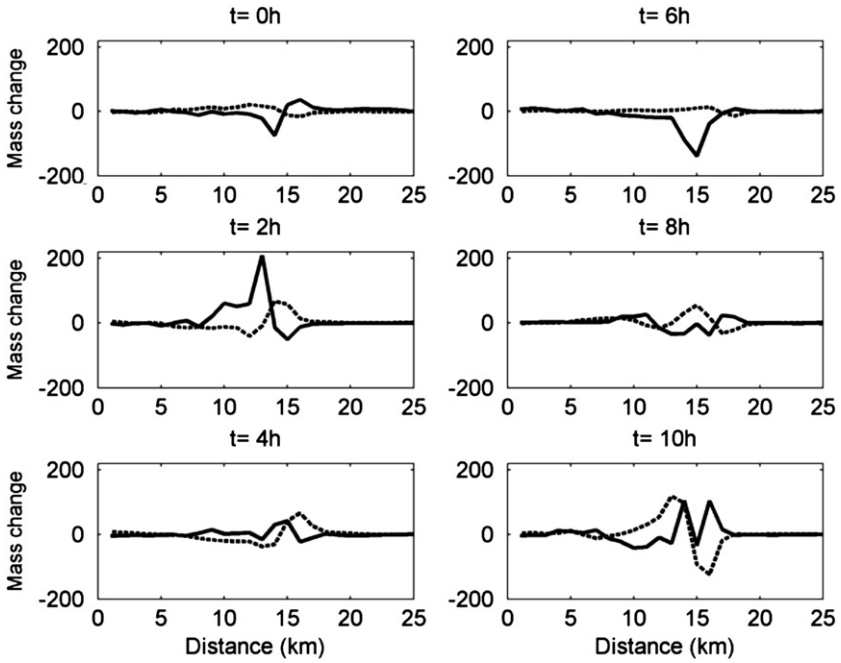

Fig. 6. Instantaneous along-channel suspended sediment budget from hour 0 to hour 10 with flocculation. The solid line denotes net deposition and the dashed line denotes horizontal advection. The mass change unit is in kg s^{-1}.

4) because strong turbulent mixing limits the floc growth. The largest flocs (200∼250 μm) are formed at slack tide before ebb (hour 6) due to strong differential settling and reduced turbulence. On ebb, due to the dominance of breakup process, the maximum floc size is only about 100 μm.

Fig. 5a shows floc size distributions near the salt front (km 14.5) and the corresponding settling flux at 0.8 m above bottom (mab). At slack tide before flood (hour 0), the SSC is low (∼0.1 kg m^{-3}) with size in the range of 30–200 μm. With increasing flood currents (hour 3), the SSC increases (∼0.4 kg m^{-3}), the floc size extends to 50∼320 μm, and D_{50}=130 μm. At slack tide before ebb (hour 6), the floc size further increases and D_{50}=210 μm, despite the relatively low SSC (∼0.1 kg m^{-3}). At ebb tide (hour 9), the floc size decreases and D_{50}=120 μm. The settling flux of particles ($w_{s,i}C_i$) varies significantly within the tidal cycle due to the floc size variations (Fig. 5b). For instance, settling flux at hour 6 is about two times larger than at hour 9 even though the floc concentration at hour 6 is comparable to that at hour 9 (Fig. 5a). The differences in settling flux contribute to the pronounced variations in SSC over a tidal cycle (Fig. 3).

To investigate the influence of the deposition flux, resuspension flux, and horizontal advective flux on the SSC variations, the suspended sediment budget in the water column is examined. Fig. 6 shows the horizontal advection ($uC_x = \delta_x \iint uC\,dy\,dz$) and the net resuspension at the bottom ($DE = \iint(-wC + E_s)dx\,dy$). Their sum gives the net mass change of suspended sediments ($C_t = \partial/\partial t \iint C\,dx\,dy\,dz$). At hour 0, advection moves sediments seaward but the deposition flux ($DE < 0$) is dominant, which causes the SSC to decrease. As currents change to flood (hour 2), the resuspension flux is about two times larger than the deposition flux, so resuspension of previously deposited particles ($DE > 0$) mainly contributes to the SSC increase. In the maximum flood (hour 4), the resuspension and deposition flux are comparable, and the advection is dominant. At end of flood (hour 6), many suspended sediments settle to the bed due to lack of resuspension. Resuspension becomes dominant again with the increasing ebb current (hour 8). At late ebb tide (hour 10), the dominant seaward advection of suspended sediments contributes to the downstream movement of SSC. Therefore, both horizontal advection and bottom resuspension are important for the ETM variations over a tidal cycle, but their relative contribution varies with the tidal phases.

3.3. Simulation without the flocculation model

We also consider a single particle size without flocculation. In this case, the settling velocity must be carefully chosen in order to create an ETM. Following Geyer (1993) and Warner et al. (2007), a dimensionless trapping length, l, is applied to estimate the settling velocity, $l = u_1 h_1 / w_s L$, where u_1 is the tidally averaged velocity at the upper layer of the salt front, h_1 is the thickness of the bottom boundary layer, and L is the width of the salt front. For $l \sim 1$, a stable well-defined ETM can be formed. Otherwise, if $l > 1$ the sediments move out of the salt front with few particles trapped, and when $l \ll 1$ all particles are trapped in a small area at the toe of the salt front. In the simulation, u_1 is about 0.22 m s^{-1}, h_1 is about 5 m, and L is about 4 km. We choose w_s=0.31 mm s^{-1}, corresponding to l=0.9. The equivalent floc size is 117 μm according to Eq. (7).

Fig. 7 shows snapshots of 1 psu isohaline, SSC, and bed thickness distributions from the non-flocculation model. The background value of SSC is about ∼0.03 kg m^{-3}. A permanent ETM is present that moves with the tidal currents. The ETM is slightly behind the salt front due to the tidal resuspension lag. The maximum SSC varies around 0.1∼0.2 kg m^{-3} with no significant changes over the tidal cycle. This differs significantly from the flocculation model in which the changes in particle size (settling velocity) cause strong tidal asymmetry in the SSC. Another major difference is the relative mass pool between the suspended and deposited sediments. In the flocculation model the suspended sediments tend to stay in the water, and the net (tidally averaged) accumulation of bottom sediment is small (Fig. 3). In contrast, in the non-flocculation model, the suspended sediments are trapped at the salt front. The rapid bottom sediment accumulation at the ETM is reflected in the much larger bed thickness. Another consequence of rapid sedimentation is that the ETM zone is narrow (∼5 km) and confined to the salt front.

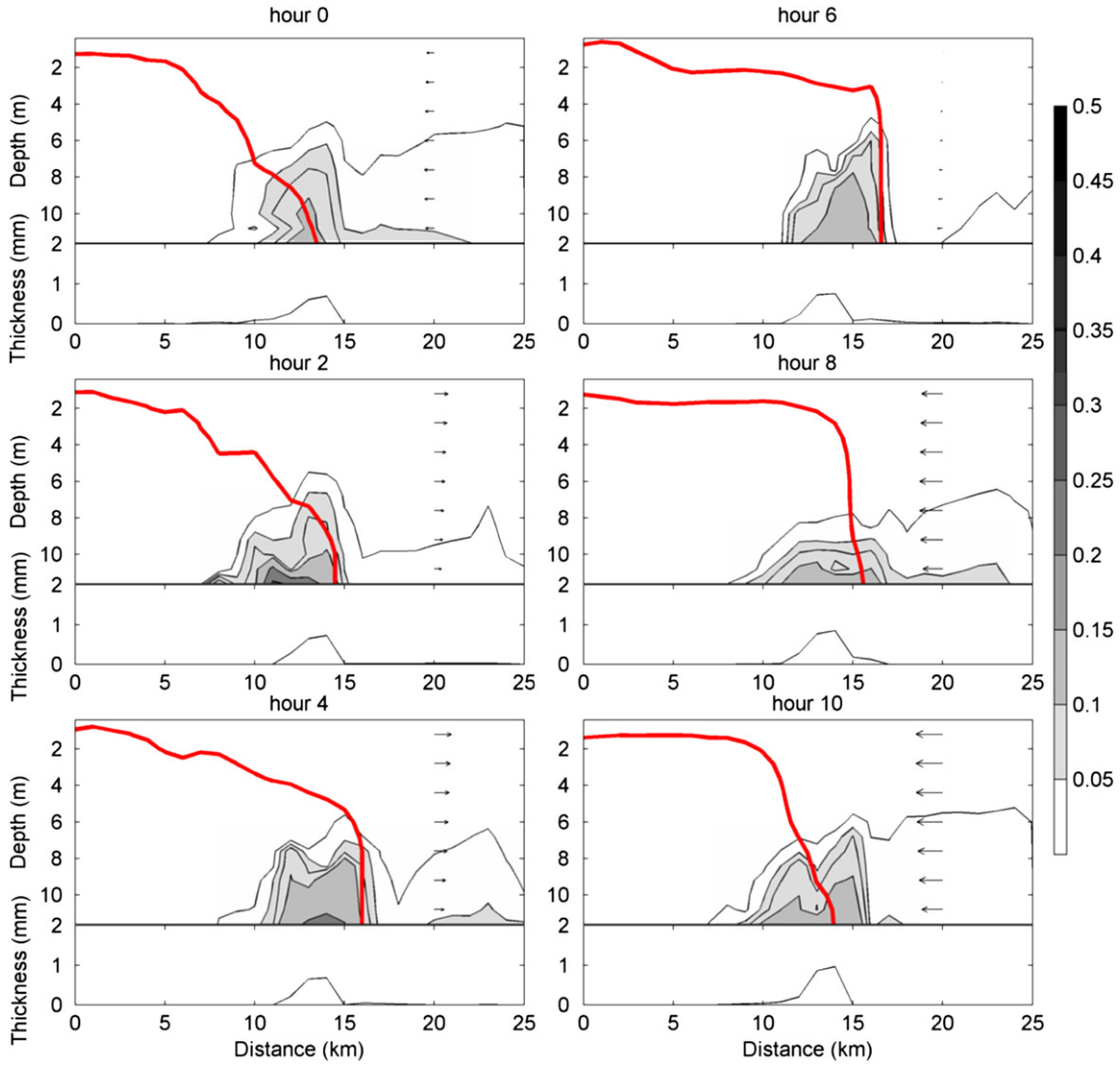

Fig. 7. Instantaneous SSC distributions with contours of 0.03, 0.05, 0.07, 0.1, 0.2, 0.3, and 0.4 kg m^{-3} (solid lines) and bed thickness (solid black line) from hour 0 to 10 without flocculation. The red line is 1 psu isohaline, and the arrows show the currents at km 20. (For interpretation of the references to color in this figure legend, the reader is referred to the web version of this article.)

4. Discussion

In the conceptual model proposed by Sanford et al. (2001), the gravitational circulation and tidal asymmetry combined with asymmetrical tidal resuspension and transport of flocs are primarily responsible for the ETM formation. At slack before flood, only the gravitational circulation exists and the mixing is weak. Most of the suspended sediments settle to the bed. On flood, strong resuspension occurs due to intensified bottom currents. Then, the suspended sediments are advected landward toward the salt front. At slack before ebb, previously resuspended particles settle near the salt front. On ebb, the sediments are resuspended again and advected seaward. Seaward of the salt front, strong stratification in the upper water column favors particle sedimentation and subsequent accumulation to the bed. The sediment will be resuspended again in the following flood, repeating the cycle. The variability of SSC in the flocculation model is consistent with the conceptual picture. Quantitatively, the SSC on flood tide is about twice larger than on ebb tide, and the ETM zone extends 10's of kilometers (Fig. 3). These results are consistent with observations in the upper Chesapeake Bay in which the observed SSC was much larger during the flood and the ETM is about 20 km wide (Sanford et al. 2001). In contrast, the non-flocculation model of Park et al. (2008) shows no obvious tidal asymmetry in the SSC and the ETM also is highly confined. We note though in nature the environmental conditions are complicated (e.g. North et al., 2004), and quantitative model evaluation can be very challenging.

Sensitivity studies are performed to investigate the influence of particle stickiness (α). The model setup is the same as in the flocculation simulation except that α is changed from 0.6 to 0.3 and 0.9, respectively. Fig. 8 compares the tidally averaged SSC distributions at different stickiness. At $\alpha=0.3$, the SSC is about 0.2 kg m^{-3}, confined to the bottom between km 4 and km 14. The median floc size is only about 50 μm with little change with tidal currents, and settling velocity is about 0.08 mm s^{-1}. Few particles are trapped at low stickiness due to smaller settling velocity. At $\alpha=0.9$, the results are similar to $\alpha=0.6$ (Base), though the suspended particles are more constrained in the salt front from km 10 to km 15. The median floc size varies from 200 to 400 μm near the salt front. Through its effect on the particle size, the particle stickiness can have significant influence on sediment trapping, especially when the stickiness is small. Sanford et al. (2001) suggested that the seasonal variations in sediment trapping

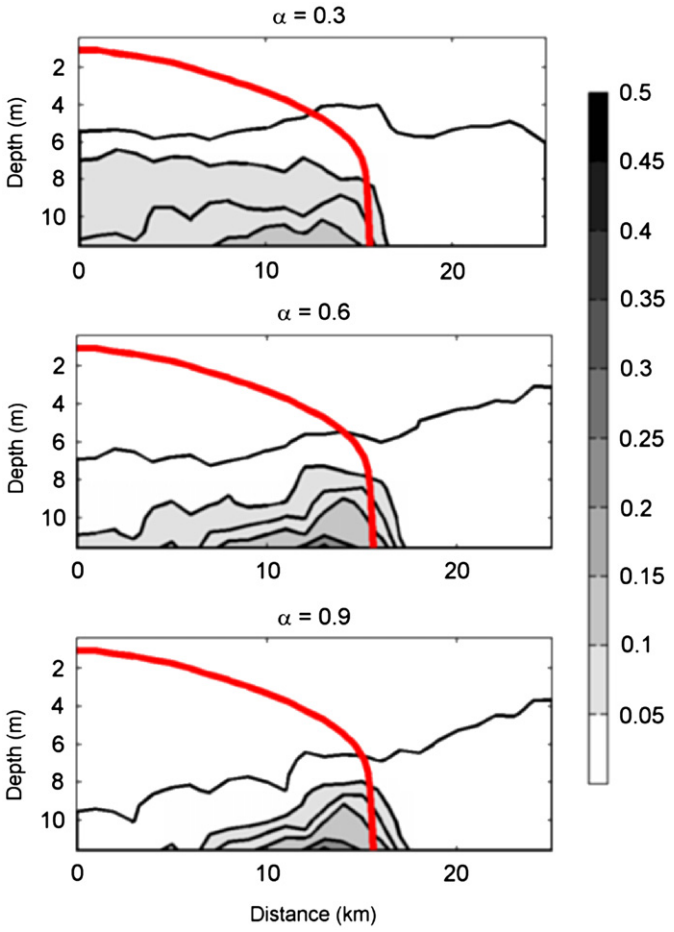

Fig. 8. The tidally averaged 1 psu isohaline (thick solid line), and SSC with contours of 0.03, 0.05, 0.07, 0.1, and 0.2 kg m^{-3} (solid lines) for different particle stickiness, 0.3, 0.6 (Base), and 0.9.

in the Upper Chesapeake Bay may be partly caused by the variations in particle organic content and hence particle stickiness.

Xu et al. (2008) tested the sensitivity of flocculation model to fractal dimension varying from 1.8 to 2.2. The increase of fractal dimension reduces the efficiency of floc breakup, which favors slightly larger floc formation. In this study, the fractal dimension is assumed to be 2.0, following Winterwerp (1998). Two model simulations were carried out with n_f=1.7 and 2.3 while keeping the other settings the same as in the base run. The results are similar to the base case (not shown), suggesting that the model is not sensitive to variations of fractal dimension over this range.

Acknowledgements

This study was supported by the New York Sea Grant Institute. We would like to thank the two anonymous reviewers assigned to the article for their comments and insights.

References

Baugh, J.V., Manning, A.J., 2007. An assessment of a new settling velocity parameterisation for cohesive sediment transport modeling. Continental Shelf Research 27, 1835–1855.

Blumberg, A.F., Mellor, G.L., 1987. A description of a three-dimensional coastal ocean circulation model. In: Heaps, N. (ed.), Three-Dimensional Coastal Ocean Models, American Geophysical Union, 208 pp.

Burchard, H., Baumert, H., 1998. The formation of estuarine turbidity maxima due to density effects in the salt wedge. A hydrodynamic process study. Journal of Physical Oceanography 28, 309–321.

Chant, R.J., Wilson, R.E., 2000. Internal hydraulics and mixing in a highly stratified estuary. Journal of Geophysical Research 105, 14,215–14,222.

Dyer, K.R., Evans, E.M., 1989. Dynamics of turbidity maximum in a homogenous tidal channel. Journal of Coastal Research SI, 23–36.

Festa, J.F., Hansen, D.V., 1978. Turbidity maxima in partially mixed estuaries. Estuarine and Coastal Marine Science 7, 347–359.

Geyer, W.R., 1993. The importance of suppression of turbulence by stratification on the estuarine turbidity maximum. Estuaries 16, 113–125.

Geyer, W.R., Signell, R., Kineke, G., 1998. Lateral trapping of sediment in a partially mixed estuaries. In: Dronkers, J., Scheffers, M. (Eds.), Physics of Estuaries and Coastal Seas: Proceedings of the 8th International Biennial Conference on Physics of Estuaries and Coastal Seas. A.A. Balkema, Rotterdam, The Netherlands, pp. 115–124.

Geyer, W.R., Hill, P.S., Kineke, G.C., 2004. The transport, transformation and dispersal of sediment by buoyant coastal flows. Continental Shelf Research 24, 927–949.

Jay, D.A., Musiak, J.D., 1994. Particle trapping in estuarine tidal flows. Journal of Geophysical Research 99, 20,445–20,461.

Lick, W., Huang, H., Jepsen, R., 1993. Flocculation of fine-grained sediments due to differential settling. Journal of Geophysical Research 98, 10279–10288.

Mellor, G.L., 1998. User's guide for a three-dimensional primitive equation numerical ocean model. Program in Atmospheric and Oceanic Sciences, Princeton University, 35 pp.

Mehta, A.J., 1986. Characterization of cohesive sediment properties and transport processes in estuaries. In: Metha (Ed.), Lecture Notes on Coastal and Estuarine Studies, 14. Springer, Berlin, pp. 290–325.

Mellor, G.L., Yamada, T., 1974. A hierarchy of turbulence closure models for planetary boundary layers. Journal of Atmospheric Science 31, 1791–1806.

North, E.W., Chao, S.-Y., Sanford, L.P., Hood, R.R., 2004. The influence of wind and river pulses on an estuarine turbidity maximum: numerical studies and field observations in Chesapeake Bay. Estuaries 27, 132–146.

Park, K., Wang, H.V., Kim, S.C., 2008. A model study of estuarine turbidity maximum along the main channel of the upper Chesapeake Bay. Estuaries and Coasts 31, 115–133.

Postma, H., 1967. Sediment transport and sedimentation in the estuarine environment. In: Lauff, G.H. (Ed.), Estuaries, 83. American Association Advanced Scientific Publication, Washington, DC, pp. 158–179.

Sanford, L.P., Dickhudt, P.J., Rubiano-Gomez, L., Yates, M., Suttles, S.E., Friedrichs, C.T., Fugate, D.D., Romine, H., 2005. Variability of suspended particle concentrations, sizes, and settling velocities in the Chesapeake Bay turbidity maximum. In: Droppo, I.G., Leppard, G.G., Liss, S.N., Milligan, T.G. (Eds.), Flocculation in Natural and Engineered Environmental Systems. CRC Press, Boca Raton, Florida, pp. 211–236.

Sanford, L.P., Suttles, S.E., Halka, J.P., 2001. Reconsidering the physics of the Chesapeake Bay estuarine turbidity maximum. Estuaries 24, 655–669.

Schubel, J.R., 1968. Turbidity maximum of the northern Chesapeake Bay. Science 161, 1013–1015.

Scully, M.E., Friedrichs, C.T., 2007. Sediment pumping by tidal asymetry in a partially mixed estuary. Journal of Geophysical Research 112, C07028.

Simenstad, C.A., Morgan, C.A., Cordell, J.R., Baross, J.A., 1994. Flux, passive retention, and active residence of zooplankton in Columbia River estuarine turbidity maxima. In: Dyer, K.R., Orth, R.J. (Eds.), Changes in Fluxesin Estuarines: Implications from Science to Management. Olsen and Olsen, Fredensborg, Denmark, pp. 473–482.

Simpson, J.H., Williams, E., Brasseur, L.H., Brubaker, J.M., 2004. The impact of tidal straining on the cycle of turbulence in a partially stratified estuary. Continental Shelf Research 25, 51–64.

Son, M., Hsu, T.J., 2008. Flocculation model of cohesive sediment using variable fractal dimension. Environmental Fluid Mechanics 8, 55–71.

Sternberg, R.W., Berhane, I., Ogston, A.S., 1999. Measurement of size and settling velocity of suspended aggregates on the northern California continental shelf. Marine Geology 154, 43–53.

Traykovski, P., Geyer, W.R., Sommerfield, C., 2004. Rapid sediment deposition and fine-scale strata formation in the Hudson estuary. Journal of Geophysical Research 109, F02004, doi:10.1029/2003JF000096.

Trowbridge, J.H., Geyer, W.R., Bowen, M.M., Williams III, A.J., 1999. Near-bottom turbulence measurements in a partially mixed estuary: turbulent energy balance, velocity structure, and along-channel momentum balance. Journal of Physical Oceanography 29, 3056–3072.

Uncles, R.J., Stephens, J.A., Law, D.J., 2006. Turbidity maximum in the macrotidal, highly turbid Humber Estuary, UK: flocs, fluid mud, stationary suspensions and tidal bores. Estuarine, Coastal and Shelf Science 67, 30–52.

Van Leussen, W., 1994. Estuarine macroflocs and their role in fine-grained sediment transport. Ph.D. Thesis, University of Utrecht, Netherlands.

Wang, D.P., 2006. Tidally generated internal waves in partially mixed estuaries. Continental Shelf Research 26, 1469–1480.

Warner, J.C., Sherwood, C.R., Geyer, W.R., 2007. Sensitivity of estuarine turbidity maximum to settling velocity, tidal mixing, and sediment supply. In: Maa, J.P.-Y., Sanford, L.P., Schoellhamer, D.H. (Eds.), Estuarine and Coastal Fine Sediments Dynamics—Proceedings in Marine Science, 8. Elsevier, Amsterdam, pp. 355–376.

Warner, J.C., Sherwood, C.R., Arango, H.G., Signell, R.P., 2005. Performance of four turbulence closure models implemented using a generic length scale method. Ocean Modelling 8, 81–113.

Winterwerp, J.C., 1998. A simple model for turbulence induced flocculation of cohesive sediment. Journal of Hydraulic Research 36, 309–326.

Winterwerp, J.C., 2002. On the flocculation and settling velocity of estuarine mud. Continental Shelf Research 22, 1339–1360.
Xie, D., Wang, Z., Gao, S., De Vriend, H.J., 2009. Modeling the tidal channel morphodynamics in a macro-tidal embayment, Hangzhou Bay, China. Continental Shelf Research 29, 1757–1767.
Xu, F., Wang, D.P., Riemer, N., 2008. Modeling flocculation processes of fine-grained particles using a size-resolved method: comparison with published laboratory experiments. Continental Shelf Research 28, 2668–2677.